Published in final edited form as:
SIAM J Appl Math. 2005 ; 65(5): 1748–1771.

EFFECTS OF SOG ON DPP-RECEPTOR BINDING*

YUAN LOU†, **QING NIE**‡, and **FREDERIC Y. M. WAN**†

† *Department of Mathematics, The Ohio State University, Columbus, OH 43210 (lou@math.ohio-state.edu)*

‡ *Department of Mathematics, Center for Complex Biology Systems, University of California, Irvine, CA 92697 (qnie@math.uci.edu, fwan@math.uci.edu)*

Abstract

Concentration gradients of morphogens are known to be instrumental in cell signaling and tissue patterning. Of interest here is how the presence of a competitor of BMP ligands affects cell signaling. The effects of Sog on the binding of Dpp with cell receptors are analyzed for dorsal-ventral morphogen gradient formation in vertebrate and *Drosophila* embryos. This prototype system includes diffusing ligands, degradation of morphogens, and cleavage of Dpp-Sog complexes by Tolloid to free up Dpp. Simple and biologically meaningful necessary and sufficient conditions for the existence of a steady state gradient configuration are established, and existence theorems are proved. For high Sog production rates (relative to the Dpp production rate), it is found that the steady state configuration exhibits a more intense Dpp-receptor concentration near the dorsal midline. Numerical simulations of the evolution of the system show that, beyond some threshold Sog production rate, the transient Dpp-receptor concentration at the dorsal midline would become more intense than that of the steady state, before subsiding and approaching a nonuniform steady state of lower magnitude. The magnitude of the transient concentration has been found to increase by several fold with increasing Sog production rate. The highly intense Dpp activity at and around the dorsal midline is consistent with available experimental observations and other analytical studies.

Keywords

morphogen gradients; reaction-diffusion; pattern formation; mathematical modeling

1. Introduction

The proper functioning of tissues and organs requires that each cell differentiate appropriately for its position. In many cases, the positional information that instructs cells about their prospective fate is conveyed by concentration gradients of morphogens bound to cell receptors. Morphogens are signaling molecules that, when bound to cell receptors, assign different cell fates at different concentrations [1], [2]. Morphogen action is of special importance in understanding development because it is a highly efficient way for a population of uncommitted cells in an embryo to create complex patterns of gene expression in space. This role of morphogens has been the prevailing thought in tissue patterning for over half a century, but only recently have there been sufficient experimental data and adequate analytical studies for us to begin to understand how various useful morphogen concentration gradients are formed [3], [4].

Dorsal-ventral (back-to-belly) patterning in vertebrate and *Drosophila* (fruit fly) embryos is now known to be regulated by bone morphogenetic proteins (BMP). The BMP activity is

*The work was partially supported by NIH grants R01GM67247, P20GM066051, and NSF SCREM grant DMS0112416.
http://www.siam.org/journals/siap/65-5/43321.html

controlled mainly by several secreted factors including the antagonists *chordin* and *short gastrulation* (Sog). In *Drosophila*, seven zygotic genes have been proposed to regulate dorsal-ventral patterning. Among them, *decapentaplegic* (Dpp) encodes BMP homologues that promote dorsal cell fates such as *amnioserosa* and inhibits development of the ventral central nervous system. The chordin homologue Sog is expressed ventrally and promotes central nervous system development. The phenotype of Sog loss-of-function mutants is intriguing; as expected for a Dpp antagonist, ventral structures are lost but, in addition, the amnioserosa is reduced. This result is paradoxical, as the amnioserosa is the dorsal-most tissue, and thus apparently a BMP antagonist is required for maximal BMP signaling [5], [6], [7], [8].

In principle, morphogen concentration gradients can be generated through the production of morphogens at particular sources, followed by their diffusion and degradation in appropriate regions [4], [9], [10], [11], [12]. In the above Dpp/Sog system, the production of Dpp is pretty much uniform in the dorsal region and absent in the ventral region, while the opposite is true for Sog. However, the Dpp activity has a sharp peak around the midline of the dorsal region in the presence of its “inhibitor” Sog. Mutation of Sog results in a reduction and a broadening of Dpp activity around the midline of the dorsal region. As the system contains many variables, the question of what leads to a sharp concentration peak is difficult to tackle by traditional experimental means.

Recently, Eldar et al. [13] studied a more complex morphogen system that includes the effects of Sog (and other morphogens) on Dpp activities. By performing massive computer calculations to search for molecular networks that support robustness, they found that the presence of the BMP inhibitor Sog stimulates intense Dpp activity at the dorsal midline resulting in highly nonuniform Dpp-receptor concentration in space for the the patterning process. They also showed that the Dpp concentration gradient itself is robust to changes in gene dosage. Two conditions were stipulated in their model to produce agreement with experimentally observed gradient formation. First, the steady state of the system is achieved by shutting off the production of Dpp through setting the production rate to zero 10 minutes after the initiation of the system [14], and there is no degradation of Dpp-receptor complex in the model. Second, the model requires immobility of free Dpp molecules; i.e., Dpp does not diffuse, but diffusion of the Dpp-Sog complexes and other ligands can occur.

For formation of morphogen gradients in a wing imaginal disc (a structure in the larva that will become the wing of the adult fly), Lander, Nie, and Wan [4] and Lou, Nie, and Wan [9] have demonstrated the important biological roles of diffusion for Dpp, and degradation for the Dpp-receptor complex. Without degradation, the steady state of the system is not achievable unless ligand production is shut off after a while, as in [14]. Eldar et al., in a recent paper [15], have also studied how degradation of ligand affects robustness of morphogen gradients. Most recently, the diffusion coefficient of Dpp has been measured *in vivo* using FCS (fluorescence correlation spectroscopy) techniques [16], and it was found that the magnitude of diffusion coefficient for Dpp is close to the magnitude of the diffusion coefficient for the Dpp-Sog complex used in [14] and hence not negligible.

Given the rather special restrictions on the Dpp/Sog system in [13] and [14], it is desirable to investigate the possibility of an alternative and simpler known biological mechanism for the generation of the intense Dpp activities around the dorsal midline. In this paper, we will extend the dynamic Dpp/Sog system formulated in [17] for morphogen activities in dorsal-ventral patterning by allowing for diffusion of ligands, degradation of the morphogens, and the cleavage of Dpp-Sog complexes by the enzyme Tolloid to free up a fraction τ of Dpp and to degrade part of Sog.

In this study, we will establish a biologically meaningful necessary and sufficient condition for the existence of a steady state. This condition requires a balance of the production of ligands, strength of degradation, and rate of cleavage of Dpp-Sog complex by Tolloid, with *no* restrictions on the diffusion coefficients of the ligands. To gain insight into the dependence of the morphogen activities on various biological parameters, we will obtain a perturbation solution of the steady state gradients with a biologically relevant assumption that the Sog production rate is high compared to that of Dpp [13], [14]. The solution indicates that the requirement for complete immobility of Dpp is not necessary for a biologically realistic Dpp-receptor gradient that is intense in Dpp activity at the dorsal midline. Finally, we will perform numerical simulations for the dynamics of the system. It is found that the cleavage of Sog-Dpp complex by Tolloid produces a transient peak of the Dpp-receptor concentration around the dorsal midline that is significantly stronger than the corresponding concentration at the steady state. The dependence of the peak on various biological parameters, including Sog production rate and diffusion coefficients, is also investigated. The overall features of the various concentrations of the model are consistent with experimental observations [5], [6], [7], [8]. A more complete model including more biological components and its comparison with new experiments on robustness of morphogen gradients will be presented in a separate paper [18].

2. Mathematical formulation

For an analytical and computational study of the biological phenomenon of interest, a system of partial differential equations and auxiliary conditions is formulated to capture the essential features of the dynamics of the two interacting morphogens. This approach was first applied to study the development of the *Drosophila* wing imaginal disc [19], [20], [4]. The three basic biological processes involving Dpp in the wing disc are diffusion for free Dpp molecules, their reversible binding with receptors, and degradation of the bound Dpp. The main purpose was to investigate the role of diffusion in the formation of a Dpp-receptor concentration gradient in the wing disc. That system was extended to include the effect of Sog on Dpp activities in a dorsal-ventral configuration [17] in an embryo, with the cleavage of Dpp-Sog complexes by Tolloid implicitly incorporated into the system through the complete recovery of Dpp after cleavage (while the Sog components degrade completely). The cleavage-recovery phenomenon has been suggested by previous experimental studies [21], [22]. Here we consider an even more general system than that in [17] by allowing fractional recovery through the fraction parameter τ, $0 \leq \tau \leq 1$, with $\tau = 1$ corresponding to complete recovery.

The setting for dorsal-ventral patterning in a *Drosophila* embryo during development is different and more complex than that considered in [4]. As shown in the sketch of the dorsal-ventral cross section of the embryo in Figure 1, Dpp is produced only in the dorsal region (with the rate $v_L(x)$), while Sog is produced only in the ventral region (with the rate $v_S(x)$). For a one-dimensional study of the dynamics of Sog and Dpp in the presence of cell receptors, we have idealized the dorsal-ventral annular cross-section of the embryo as a ring and introduced an artificial cut of the ring at the ventral midline to map the cut ring onto the line segment $[-X_{\max}, X_{\max}]$, with $X = 0$ corresponding to the dorsal midline. Let [L], [S], [LS], [LR] denote the concentrations of Dpp, Sog, Dpp-Sog complexes, and Dpp bound to receptors, respectively. The first three diffuse with coefficients of diffusion D_L, D_S, and D_{LS}, respectively, while the concentration for the immobile and undegradable receptor is fixed at R_0 and uniformly distributed in $[-X_{\max}, X_{\max}]$. The system of equations governing the morphogen dynamics of such a system consists of the following four coupled second order differential equations, three of them being nonlinear partial differential equations (PDE) of the reaction-diffusion type:

$$\frac{\partial[\mathrm{L}]}{\partial T} = D_{\mathrm{L}}\frac{\partial^2[\mathrm{L}]}{\partial X^2} - K_{\mathrm{on}}[\mathrm{L}](R_0 - [\mathrm{LR}]) - \mathcal{J}_{\mathrm{on}}[\mathrm{L}][\mathrm{S}] + K_{\mathrm{off}}[\mathrm{LR}] + (\mathcal{J}_{\mathrm{off}} + \tau\mathcal{J}_{\mathrm{deg}})[\mathrm{LS}] + v_L(X), \tag{1}$$

$$\frac{\partial[\mathrm{LR}]}{\partial T} = K_{\mathrm{on}}[\mathrm{L}](R_0 - [\mathrm{LR}]) - (K_{\mathrm{off}} + K_{\mathrm{deg}})[\mathrm{LR}], \tag{2}$$

$$\frac{\partial[\mathrm{LS}]}{\partial T} = D_{\mathrm{LS}}\frac{\partial^2[\mathrm{LS}]}{\partial X^2} + \mathcal{J}_{\mathrm{on}}[\mathrm{L}][\mathrm{S}] - (\mathcal{J}_{\mathrm{off}} + \mathcal{J}_{\mathrm{deg}})[\mathrm{LS}], \tag{3}$$

$$\frac{\partial[\mathrm{S}]}{\partial T} = D_{\mathrm{S}}\frac{\partial^2[\mathrm{S}]}{\partial X^2} - \mathcal{J}_{\mathrm{on}}[\mathrm{L}][\mathrm{S}] + \mathcal{J}_{\mathrm{off}}[\mathrm{LS}] + v_S(X) \tag{4}$$

for $-X_{\max} < X < X_{\max}$ and $T > 0$. The coefficients $\{K_{on}, J_{on}\}$, $\{K_{off}, J_{off}\}$, $\{K_{deg}, J_{deg}\}$ are the binding rate constants, the off rate constants, and the degradation rate constants of Dpp and Sog, respectively. With the morphogen activities symmetric about the ventral (as well as dorsal) midline, we must have the following symmetry (no flux) conditions at the two ends of the solution domain:

$$X = \pm X_{\max} : \frac{\partial[L]}{\partial X} = \frac{\partial[LS]}{\partial X} = \frac{\partial[S]}{\partial X} = 0.$$

The number of independent parameters may be reduced by suitable normalization. Let

$$x = \frac{X}{X_{\max}}, \quad t = \frac{D_0 T}{X_{\max}^2}, \tag{5}$$

$$\{h_L, h_{LS}\} = \frac{X_{\max}^2 R_0}{D_0}\{K_{on}, \mathcal{J}_{on}\}, \tag{6}$$

$$\{f_L, f_{LS}, g_L, g_{LS}\} = \frac{X_{\max}^2}{D_0}\{K_{\mathrm{off}}, \mathcal{J}_{\mathrm{off}}, K_{\mathrm{deg}}, \mathcal{J}_{\mathrm{deg}}\}, \tag{7}$$

$$\{V_L(x), V_S(x)\} = \frac{X_{\max}^2}{R_0 D_0}\{v_L(X), v_S(X)\}, \tag{8}$$

$$\{\rho_L, \rho_S, \rho_{LS}\} = \left\{\frac{D_L}{D_0}, \frac{D_{LS}}{D_0}, \frac{D_S}{D_0}\right\}, \tag{9}$$

$$\{A, B, C, D\} = \left\{\frac{[\mathrm{L}]}{R_0}, \frac{[\mathrm{LR}]}{R_0}, \frac{[\mathrm{LS}]}{R_0}, \frac{[\mathrm{S}]}{R_0}\right\}. \tag{10}$$

In these relations, it would seem natural to choose the normalizing diffusion coefficient D_0 to be the maximum of the three diffusion coefficients. However, it turns out to be more appropriate to choose $D_0 = D_S$ to facilitate an appreciation of the implication of the solution. At this time, we will leave D_0 unspecified, but will see in section 4 why it is expeditious to specify it as D_S. In terms of these normalized quantities, (1)–(4) may be written as

$$A_{,t} = \rho_L A_{,xx} - h_L A(1 - B) - h_{LS} AD + f_L B + (f_{LS} + \tau g_{LS})C + V_L(x), \tag{11}$$

$$B_{,t} = h_L A(1 - B) - (f_L + g_L)B, \tag{12}$$

$$C_{,t} = \rho_{LS} C_{,xx} + h_{LS} AD - (f_{LS} + g_{LS})C, \tag{13}$$

$$D_{,t} = \rho_S D_{,xx} - h_{LS} AD + f_{LS} C + V_S(x) \tag{14}$$

for $-1 < x < 1$ and $t > 0$, with $(\,)_{,z} = \partial(\,)/\partial z$ for the temporal and spatial derivatives of the dependent variables *A, B, C, D*.

3. Existence of steady state solutions

In this section, we examine the existence of time-independent (or steady state) solutions of the system (11)–(14) subject to the no flux conditions at the two end points, which can now be written in terms of the normalized unknowns as

$$x = \pm 1: \quad A_{,x} = C_{,x} = D_{,x} = 0 \quad (t > 0). \tag{15}$$

With the steady state solution independent of time, (12) becomes an algebraic equation and can be solved for B in terms of A:

$$B = \frac{A}{a_L + A}, \quad a_L = \frac{g_L + f_L}{h_L}. \tag{16}$$

The expression for *B* is then used to eliminate it from (11), leaving the following three simultaneous equations for the three unknowns *A*, *C*, and *D*:

$$\rho_L A_{,xx} - \frac{g_L h_L A}{f_L + g_L + h_L A} - h_{LS} AD + (f_{LS} + \tau g_{LS})C + V_L = 0, \tag{17}$$

$$\rho_{LS} C_{,xx} + h_{LS} AD - (f_{LS} + g_{LS})C = 0, \tag{18}$$

$$\rho_S D_{,xx} - h_{LS} AD + f_{LS} C + V_S = 0 \tag{19}$$

for $-1 < x < 1$ subject to the boundary conditions (15).

Throughout this section we assume the following:

(A1) f_L, f_{LS}, g_L, g_{LS}, h_L, and h_{LS} are continuous positive functions in $[-1, 1]$;ρ_L, ρ_{LS}, and ρ_S are positive constants; V_S, V_L are nonnegative integrable functions that satisfy $\int_{-1}^{1} V_L > 0$ and $\int_{-1}^{1} V_S > 0$; and τ is a constant satisfying $0 \le \tau \le 1$.

If $V_L(x)$ and $V_S(x)$ are continuous, we seek a classical solution of (15)–(19); i.e., *A*, *C*, and *D* are twice continuously differentiable in $[-1, 1]$ that satisfy (15)–(19).

Theorem 3.1

Suppose that (A1) *holds and* V_L, V_S *are continuous in* $[-1, 1]$. *Then* (15)–(19) *has a positive classical solution if and only if both of the following inequalities hold:*

$$\int_{-1}^{1} V_L(x)dx > (1 - \tau)\int_{-1}^{1} V_S(x)dx, \tag{20}$$

$$\int_{-1}^{1} V_L(x)dx < (1-\tau)\int_{-1}^{1} V_S(x)dx + \int_{-1}^{1} g_L(x)dx. \tag{21}$$

Since $\int_{-1}^{1} V_L(x) > 0$, the first condition is trivially satisfied for $\tau = 1$ (full recovery of Dpp), and the second is a distributed version of the necessary and sufficient condition for existence in [9], [10], [11], [12] (that the Dpp production rate must be slower than the degradation rate of the Dpp-receptor complexes). For $0 \le \tau < 1$, these two conditions may be combined to give a similar condition on a nonnegative "effective" Dpp production rate $[V_L - (1 - \tau)V_S]$ (see section 5).

Lemma 3.2

If (15)–(19) *has a positive classical solution, then* (20) *and* (21) *must hold.*

Proof—Adding up (17) and (18) and integrating over [−1, 1], we obtain with the help of (15)

$$\int_{-1}^{1} V_L = \int_{-1}^{1} \frac{g_L h_L A}{f_L + g_L + h_L A} + (1-\tau)\int_{-1}^{1} g_{LS} C. \tag{22}$$

Similarly, adding up (18) and (19) and integrating over [−1, 1], we get

$$\int_{-1}^{1} g_{LS} C = \int_{-1}^{1} V_S. \tag{23}$$

It follows from (22) and (23) that

$$\int_{-1}^{1} V_L = \int_{-1}^{1} \frac{g_L h_L A}{f_L + g_L + h_L A} + (1-\tau)\int_{-1}^{1} V_S. \tag{24}$$

For $A > 0$ in [−1, 1], we have

$$0 < \int_{-1}^{1} \frac{g_L h_L A}{f_L + g_L + h_L A} < \int_{-1}^{1} g_L, \tag{25}$$

which along with (24) implies (20)–(21).

In view of Lemma 3.2, we'll assume that (20)–(21) holds for the rest of this subsection. Our goal is to show that if V_L and V_S are continuous, then the condition (20)–(21) implies that (15)–(19) has at least a positive classical solution. The idea is to introduce some parameter and consider the following system of equations:

$$\rho_L A_{,xx} + \lambda F_1(x, A, C, D) = 0, \quad -1 < x < 1, \tag{26}$$

$$\rho_{LS} C_{,xx} + \lambda F_2(x, A, C, D) = 0, \quad -1 < x < 1, \tag{27}$$

$$\rho_S D_{,xx} + \lambda F_3(x, A, C, D) = 0, \quad -1 < x < 1, \tag{28}$$

$$A_{,x} = C_{,x} = D_{,x} = 0 \text{ at } x = -1, 1, \tag{29}$$

where $\lambda \in (0, 1]$ and F_i $(i = 1, 2, 3)$ is given by

$$F_1(x, \tilde{A}, \tilde{C}, \tilde{D}) = -\frac{g_L h_L \tilde{A}}{f_L + g_L + h_L \tilde{A}} - h_{LS}\tilde{A}\tilde{D} + (f_{LS} + \tau g_{LS})\tilde{C} + V_L, \tag{30}$$

$$F_2(x, \tilde{A}, \tilde{C}, \tilde{D}) = h_{LS}\tilde{A}\tilde{D} - (f_{LS} + g_{LS})\tilde{C}, \tag{31}$$

$$F_3(x, \tilde{A}, \tilde{C}, \tilde{D}) = -h_{LS}\tilde{A}\tilde{D} + f_{LS}\tilde{C} + V_S. \tag{32}$$

We establish some a priori estimates for nonnegative classical solutions of (26)–(29).

LEMMA 3.3

Let $(\tilde{A}, \tilde{C}, \tilde{D})$ *be any nonnegative classical solution of* (26)–(29). *If* $\lambda > 0$, *then* $\tilde{A}(x) > 0$, $\tilde{C}(x) > 0$, *and* $D(x) > 0$ *for every* $x \in [-1, 1]$.

Proof—Similar to (23) we have $\int_{-1}^{1} g_{LS}\tilde{C} = \int_{-1}^{1} V_S$. Hence $\tilde{C} \geq 0$, $\tilde{C} \not\equiv 0$. By (27) and (31) we have

$$-\rho_{LS}\tilde{C}_{,xx} + \lambda(f_{LS} + g_{LS})\tilde{C} = \lambda h_{LS}\tilde{A}\tilde{D} \geq 0, \quad -1 < x < 1. \tag{33}$$

This together with $\tilde{C}_{,x}(-1) = \tilde{C}_{,x}(1) = 0$, via the maximum principle [23], implies that $\tilde{C}(x) > 0$ for every $x \in [-1, 1]$. Since $V_L \not\equiv 0$ and $V_S \not\equiv 0$, similarly by (26)–(29) and the maximum principle we can show that $\tilde{A} > 0$ and $D > 0$ in $[-1, 1]$.

LEMMA 3.4

There exists some constant $M > 0$, *independent of* λ, *such that for any* $0 < \lambda \leq 1$ *and any positive classical solution* $(\tilde{A}, C, D)$ *of* (26)–(29) *we have*

$$\|\tilde{A}\|_{L^\infty} + \|\tilde{C}\|_{L^\infty} + \|\tilde{D}\|_{L^\infty} \leq M. \tag{34}$$

The proof of Lemma 3.4 is postponed to the appendix. Lemmas 3.3 and 3.4 enable us to define Leray–Schauder degree (see, e.g., [24]) for a certain operator whose Fixed points correspond to positive solutions of (26)–(29).

Set $E = \{C[-1, 1]\}^3$ and $C_N^2[-1, 1] = \{u \in C^2[-1, 1] : u_{,x}(-1) = u_{,x}(1) = 0\}$. For any positive constant γ, let L_γ^{-1} denote the inverse of the operator $L_\gamma := -\gamma\frac{d^2}{dx^2} + I : C_N^2[-1, 1] \to C[-1, 1]$, where I denotes the identity map from $C[-1, 1]$ to itself.

For every $\lambda \in [0, 1]$, define operator $T(\lambda): E \to E$ by

$$T(\lambda)(\tilde{A}, \tilde{C}, \tilde{D}) = \begin{pmatrix} L_{\rho_L}^{-1}[\tilde{A} + \lambda F_1^+(x, \tilde{A}, \tilde{C}, \tilde{D})] \\ L_{\rho_{LS}}^{-1}[\tilde{C} + \lambda F_2(x, \tilde{A}, \tilde{C}, \tilde{D})] \\ L_{\rho_S}^{-1}[\tilde{D} + \lambda F_3(x, \tilde{A}, \tilde{C}, \tilde{D})] \end{pmatrix}, \tag{35}$$

where

$$F_1^+(x, \tilde{A}, \tilde{C}, \tilde{D}) = \frac{-g_L h_L A}{f_L + g_L + h_L A_+} - h_{LS} AD + (f_{LS} + \tau g_{LS})C + V_L, \tag{36}$$

$A_+ = \max(A, 0)$. By standard regularity theory and the embedding theorem, we see that $T(\lambda)$ is well defined and continuous, and the operator T: $[-1, 1] \times E \to E$, defined by $T(\lambda, \tilde{A}, C, D) = T(\lambda)(\tilde{A}, C, D)$, is continuous and compact. For M given in (34), define

$$\Omega = \{(\tilde{A}, \tilde{C}, \tilde{D}) \in E : 0 < \tilde{A}(x), \tilde{C}(x), \tilde{D}(x) < M + 1 \ \forall\ x \in [-1, 1]\}.$$

Ω is an open and bounded subset of E. By Lemmas 3.3 and 3.4, we see that for any $\lambda \in (0, 1]$, $[I - T(\lambda)]^{-1}\{(0, 0, 0)\} \notin \partial\Omega$. Hence the Leray–Schauder degree, deg $(I - T(\lambda), \Omega, (0, 0, 0))$, is well defined for $0 < \lambda \leq 1$. Moreover, by the homotopy invariance of the Leray–Schauder degree [24], deg $(I - T(\lambda), \Omega, (0, 0, 0))$ is a constant function for $0 < \lambda \leq 1$. To complete the proof of Theorem 3.1, we need the following result.

PROPOSITION 3.5

There exists $\delta > 0$ *such that* deg $(I - T(\lambda), \Omega, (0, 0, 0)) = 1$ *for* $\lambda \in (0, \delta)$.

The detail of the proof of this proposition is not particularly relevant to the proof of Theorem 3.1 and will be given in an appendix of this paper. Assuming Proposition 3.5, we can now complete the proof of Theorem 3.1.

Proof of Theorem 3.1—By Lemma 3.2, it suffices to establish the sufficiency part. By Proposition 3.5, for every $0 < \lambda \leq 1$, deg $(I - T(\lambda), \Omega, (0, 0, 0)) = 1$. In particular, deg $(I - T(1), \Omega, (0, 0, 0)) \neq 0$. This implies that there exists $(\tilde{A}, C, D) \in \Omega$ such that $(I - T(1))(\tilde{A}, C, D) = (0, 0, 0)$. By standard regularity theory we see that $\tilde{A}, C, D \in C^2[-1, 1]$ and is thus a positive classical solution of (15)–(19).

Specific morphogen systems of interest include those with morphogen production rates that are discontinuous in the spatial variable (see section 4). When V_L and V_S are bounded and measurable, we will be seeking $C^{1,1}$ solutions of (15)–(19), i.e., functions A, C, D that are differentiable in $[-1, 1]$; have derivatives $A_{,x}$, $C_{,x}$, and $D_{,x}$ Lipschitz continuous in $[-1, 1]$; and satisfy (15) and for every $x \in [-1, 1]$

$$\rho_L A_{,x} + \int_{-1}^{x} F_1 = \rho_{LS} C_{,x} + \int_{-1}^{x} F_2 = \rho_S D_{,x} + \int_{-1}^{x} F_3 = 0. \tag{37}$$

THEOREM 3.6

Suppose that (A1) *holds and that* V_L *and* V_S *are bounded measurable. Then* (15)–(19) *has a positive* $C^{1,1}$ *solution if and only if* (20)–(21) *holds.*

Proof—Suppose that (15)–(19) has a positive $C^{1,1}$ solution. Setting $x = 1$ in (37) and applying the same argument as in the proof of Lemma 3.2, we see that (20)–(21) must hold. On the other hand, if (20)–(21) holds, we can choose a uniformly bounded sequence of continuous positive functions $V_L^n(x)$ and $V_S^n(x)$ such that $V_L^n(x) \to V_L$ and $V_S^n(x) \to V_S$ a.e., and $0 < \int_{-1}^{1}[V_L^n - (1 - \tau)V_S^n] < \int_{-1}^{1} g_L$. By Theorem 3.1 (17)–(19), with V_L and V_S being replaced by V_L^n and V_S^n, respectively, there is a sequence of positive classical solutions, denoted by A^n, C^n, and D^n. As for Lemma 3.4, we can show that there exists some positive constant M, independent of n, such that $\|A_n\|_{L^\infty} + \|C_n\|_{L^\infty} + \|D_n\|_{L^\infty} \leq M$. Furthermore, $\|A_{,xx}^n\|_{L^\infty}$, $\|C_{,xx}^n\|_{L^\infty}$, and $\|C_{,xx}^n\|_{L^\infty}$ are uniformly bounded. By passing to a

subsequence if necessary, (A^n, C^n, D^n) converge to some functions (A,C,D) in C^1, and A,C,D satisfy (15) and are nonnegative solutions of (37). From (37) we see that $A_{,x}$, $C_{,x}$,$D_{,x}$ are Lipschitz continuous in [−1, 1]. By similar argument as in Lemma 3.3 (but instead using the maximum principle for weak solutions of (15)–(19)), we see that A,C,D are all positive in [−1, 1]. This completes the proof of Theorem 3.6.

Remark 3.7—Note that $C \in C^2[-1, 1]$. If V_L and V_S are piecewise continuous, then A and D are also piecewise twice continuously differentiable in [−1, 1].

4. Approximate steady state solutions for $V_L \ll V_S$

In previous studies [13], [14], the constant (in both space and time) Dpp production rate, $\bar{v}_L$, in the dorsal region was estimated to be significantly smaller than the constant Sog production rate, $\bar{v}_S$, in the ventral region. In [14], the ratio of the two production rates, defined as $\varepsilon \equiv \bar{v}_L/\bar{v}_S$, is 0.008 for its baseline study. The robustness of the solutions with respect to variations of $\bar{v}_S$ is studied for fixed $\bar{v}_L$ [13].

For $\bar{v}_L \ll \bar{v}_S$, so that $\varepsilon \ll 1$, we obtain below a perturbation solution for the steady state of (15)–(19), with $\tau = 1$ for simplicity. For $\tau < 1$, perturbation solution procedure applies only if (20)–(21) hold. Similar to [14], we assume

$$V_L(x) = \mathcal{V}_L H\left(\frac{1}{2} - x\right), \quad V_S(x) = \mathcal{V}_S H\left(x - \frac{1}{2}\right), \tag{38}$$

where $(\mathcal{V}_L, \mathcal{V}_S) = (v_L, v_S) X_{\max}^2 / (R_0 D_0)$ and $H(z)$ is the unit step function.

With $\bar{V}_L \ll \bar{V}_S$, we expect $D(x)$, $C(x) = O(\bar{V}_S)$, $O(\bar{V}_S)$, although the latter may be a smaller fraction of $\bar{V}_S$. On the other hand, we have $A(x) = O(\bar{V}_L)$ at most, in fact quite a bit smaller since free Dpp should eventually be bound to Sog or receptors, given that Sog is produced at a much higher rate. For these reasons, we set

$$A(x) = \frac{\mathcal{V}_L}{\mu_L^2} a(x), \quad C(x) = \frac{\mathcal{V}_S}{f_{LS} + g_{LS}} c(x), \quad D(x) = \mathcal{V}_S d(x), \tag{39}$$

where $\mu_L^2 = g_L / a_L$ and $a_L = (f_L + g_L)/h_L$. Then (17)–(19) become

$$\frac{\mathcal{V}_L}{\mathcal{V}_S}\left[\frac{\rho_L}{\mu_L^2} a'' - \frac{a}{1 + \beta_L a} + H\left(\frac{1}{2} - x\right)\right] - \mu_D^2 a d + c = 0, \tag{40a}$$

$$\rho_{LS} c'' + (f_{LS} + g_{LS})[\mu_D^2 a d - c] = 0, \tag{40b}$$

$$\rho_S d'' - [\mu_D^2 a d - c] - (1 - \sigma_{LS}) c + H\left(x - \frac{1}{2}\right) = 0, \tag{40c}$$

where $()' = d()/dx$, $\beta_L = \bar{V}_L/g_L$, $\sigma_{LS} = f_{LS}/(f_{LS}+g_{LS}) < 1$, and $\mu_D^2 = h_{LS} a_L \mathcal{V}_L / g_L$. Using symmetry about $x = 0$, we need only to consider solutions for $0 < x < 1$ with the boundary conditions at $x = 0$ being again no flux for all three unknowns a, b, and c.

The form of (40a)–(40c) suggests that we seek a perturbation solution of $\{a, c, d\}$ in ε:

$$\{a(x;\varepsilon),\ c(x;\varepsilon),\ d(x;\varepsilon)\} = \sum_{n=0}^{\infty} \{a_n(x),\ c_n(x),\ d_n(x)\}\varepsilon^n. \tag{41}$$

For moderate values of $\bar{V}_L$ so that μ_D^2 is *not* small compared to unity, the three leading term coefficients are determined by

$$\mu_D^2 a_0 d_0 - c_0 = 0, \tag{42a}$$

$$\rho_{LS} c_0'' + (f_{LS} + g_{LS})[\mu_D^2 a_0 d_0 - c_0] = 0, \tag{42b}$$

$$\rho_S d_0'' - [\mu_D^2 a_0 d_0 - c_0] - (1 - \sigma_{LS}) c_0 + H\left(x - \frac{1}{2}\right) = 0. \tag{42c}$$

The complementary case, $\mu_D^2 \ll 1$, can also be analyzed but is not relevant for our biological system.

Upon combining (42a) and (42b) we get

$$\rho_{LS} c_0'' = 0. \tag{43}$$

The no flux boundary conditions at $x = 0, 1$ require $c_0(x) \equiv \sigma_0$ for some constant σ_0. To determine σ_0, we note that (23) is still valid and requires

$$\frac{1}{2} V_S = \int_0^1 V_s(x)dx = g_{LS}\int_0^1 C(x)dx = V_S \frac{g_{LS}}{f_{LS} + g_{LS}} \int_0^1 c(x)dx \tag{44}$$

so that $\sigma_0 = 1/2(1 - \sigma_{LS})$, i.e.,

$$(1 - \sigma_{LS}) c_0(x) = \frac{1}{2}, \quad 0 \le x \le 1. \tag{45}$$

To determine $d_0(x)$, we use (42a) and (42c) to obtain

$$\rho_S d_0'' - (1 - \sigma_{LS}) c_0 + H\left(x - \frac{1}{2}\right) = 0. \tag{46}$$

Upon integration and application of boundary conditions at $x = 0, 1$, as well as the continuity condition at $x = 1/2$ for d_0, we obtain

$$\rho_S d_0(x) = \begin{cases} \delta_0 + \dfrac{x^2}{4} & \left(x \le \dfrac{1}{2}\right), \\ \delta_0 - \dfrac{1}{8} + \dfrac{1}{2}\left(x - \dfrac{x^2}{2}\right) & \left(x \ge \dfrac{1}{2}\right), \end{cases} \tag{47}$$

where δ_0 is an undetermined constant. By (42a) we have also

$$\frac{1 - \sigma_{LS}}{\rho_S} \mu_D^2 a_0(x) = \frac{1 - \sigma_{LS}}{\rho_S} \frac{c_0(x)}{d_0(x)} = \begin{cases} \dfrac{1}{2} \dfrac{1}{(\delta_0 + \frac{1}{4}x^2)} & \left(x < \dfrac{1}{2}\right), \\ \dfrac{1}{2} \dfrac{1}{[\delta_0 - \frac{1}{8} + \frac{1}{2}x - \frac{1}{4}x^2]} & \left(x > \dfrac{1}{2}\right). \end{cases} \tag{48}$$

It is rather fortuitous to have $a_0'(0) = a_0'(1) = 0$ because d_0 and c_0 satisfy no flux conditions at the two end points so that there are no boundary layers adjacent to the two ends.

It remains to determine δ_0. We note that (24) still holds, particularly when $\tau = 1$. In that case, (24) becomes

$$G(\delta_0) \equiv \int_0^1 \frac{a_0(x)}{1+\beta_L a_0(x)}dx = \frac{1}{2}. \tag{49}$$

It is easy to see that $G(\delta_0)$ is strictly monotone decreasing in δ_0 and that $G(\delta_0) \to 0$ as $\delta_0 \to \infty$. Hence $G(\delta_0) = \frac{1}{2}$ has at most one positive root, and it has one positive root if and only if $G(0) > \frac{1}{2}$. Note that $G(0)$ can be explicitly computed, and thus $G(\delta_0) = \frac{1}{2}$ determines δ_0.

Altogether, we have as the corresponding leading terms for the concentrations

$$A(x) \sim \frac{(1-\sigma_{LS})\mu_D^2 a_0(x)/\rho_S}{R_0 \mathcal{J}_{on,\mathrm{eff}}/(D_S/X_{\max}^2)}, \tag{50}$$

$$B(x) \sim \frac{\Gamma_{LS}(1-\sigma_{LS})\mu_D^2 a_0(x)/\rho_S}{1+\Gamma_{LS}(1-\sigma_{LS})\mu_D^2 a_0(x)/\rho_S}, \tag{51}$$

$$C(x) \sim \frac{1}{2}\frac{\nu_S}{\mathcal{J}_{\mathrm{deg}} R_0}, \tag{52}$$

$$D(x) \sim \frac{\nu_S/R_0}{D_S/X_{\max}^2}[\rho_S d_0(x)], \tag{53}$$

where

$$K_{on,\mathrm{eff}} \equiv \frac{K_{\mathrm{deg}} K_{on}}{K_{\mathrm{deg}}+K_{\mathrm{off}}}, \quad \mathcal{J}_{on,\mathrm{eff}} \equiv \frac{\mathcal{J}_{\mathrm{deg}}\mathcal{J}_{on}}{\mathcal{J}_{\mathrm{deg}}+\mathcal{J}_{\mathrm{off}}}, \quad \Gamma_{LS} = \frac{K_{on,\mathrm{eff}}}{\mathcal{J}_{on,\mathrm{eff}}}\frac{D_S}{K_{\mathrm{deg}} X_{\max}^2}. \tag{54}$$

In Figure 2, the perturbation solutions (50)–(53) are plotted against the numerical solutions obtained through temporal evolution (which will be discussed in the next section). The relative difference between the two solutions is 1.5% for A, 1.4% for B, 4.3% for C, and 2.9% for D for $\varepsilon = \bar{\nu}_L/\bar{\nu}_S = 0.0133$ and $\mu_D^2 = 18.4$. This illustrates the approximation and accuracy of the perturbation solution for $\varepsilon \ll 1$.

More interesting is the dependence of the leading term solutions (51)–(53) on the biological parameters. The simplest of the four is the uniformly distributed concentration of Dpp-Sog complexes in (53): it depends only on the production rate of Sog per receptor, which is uniform in the ventral region. Free Sog $D(x)$ is proportional to the quadratic function defined in (47) with a magnitude of $\bar{\nu}_S/R_0$ modified by the diffusion coefficient of Sog. That $D(x)$ is inversely proportional to D_S is not surprising, since faster diffusion of Sog would move more of it into the dorsal region for binding with the available Dpp there. Note that $\rho_S d_0(x)$ is independent of the choice of normalizing diffusion coefficient D_0 and the effects of all biological parameters are felt by $\rho_S d_0(x)$ only implicitly through the parameter δ_0.

Less expected is the dependence of $A(x)$ and $B(x)$ on the biological parameters. From (51), we see that if $\Gamma_{LS} = O(1)$, the amplitude of $B(x)$ is determined mainly by Γ_{LS}. For $\Gamma_{LS} \gg 1$, we have $B(x) \sim 1$, except possibly for a region adjacent to the ventral midline $x = 1$. In either case, the amplitude of $B(x)$ does not depend explicitly on either of the two production rate parameters $\bar{v}_S/R_0$ or $\bar{v}_L/R_0$; the effects of these two parameters on $B(x)$ are felt only through δ_0.

The situation is similar for $A(x)$. It seems unreasonable that $A(x)$ does not tend to zero with $\bar{v}_L/R_0$ (with the same observation applied to $B(x)$ as well). However, we see from a closer examination of (40a) that $\mu_D^2 = h_{LS} a_L \nabla_L / g_L$ tends to zero with $\bar{v}_L/R_0$. For sufficiently small $\bar{v}_L/R_0$, the first approximation relation (42a) would give $c_0(x) = 0$. In that case, $c(x)$ should be rescaled (by an additional factor μ_D^2) for a proper perturbation solution, while the solution of this section ceases to be applicable. In other words, to apply the perturbation solution $\{a_0(x), c_0(x), d_0(x)\}$ obtained above, we must have $\bar{v}_L/R_0$ sufficiently small so that $\bar{V}_L \bar{V}_S = \bar{v}_L/\bar{v}_S \ll 1$ but not too small so that $\mu_D^2 = h_{LS} a_L \nabla_L / g_L$ is *not* small compared to unity.

5. Numerical solutions for evolutions

The system (1)–(4) can be solved by finite difference schemes [25]. The diffusion terms are approximated by the second order central difference. The temporal evolution is approximated through the fourth order Adams–Moulton predictor-corrector method. The overall accuracy for the method is second order in space and fourth order in time.

For a typical calculation, the time step is chosen to be $\Delta t = 2 \times 10^{-4}$ seconds, and the number of points to discretize the entire dorsal and ventral region is $N = 64$. Smaller time step and larger number of points have been used to check the accuracy and convergence of the calculations.

Similar to [13], the span of both the dorsal region and the ventral region is chosen to be 175μm, i.e., $X_{max} = 175\mu$m. Unlike [13], the diffusion constants for Dpp, Sog, and Dpp-Sog are taken to be the same with $D_0 = D_L = D_{LS} = D_S = 20\mu\text{m}^2/\text{second}$ [4], so that $\rho_L = \rho_S = \rho_{LS} = 1$ (except for changes indicated in Figures 7 and 8). In this study, the synthesis rates for Dpp and Sog remain the same for all time. In particular, $v_L(X)$ is always chosen to be a nonzero constant, $\bar{v}_L$, in the dorsal region and zero in the ventral region, while $v_S(X)$ is the opposite, with $v_S(X) = \bar{v}_S$ in the ventral and zero in the dorsal region.

The dynamics of the system without Sog is very similar to that in [4], even though the ligand is produced from a localized source in [4] while the ligand is produced in the whole dorsal region for the system (1)–(4). For realistic ranges of the biological parameters of the problem, this system typically evolves quickly and monotonically to a steady state within a half hour, with the Dpp-receptor concentration almost uniform around the dorsal region. This behavior is consistent with the experimental observation of [8]. At $x = 0$ the steady state is approximately equal to $\bar{v}_L/(K_{deg}R_0)$.

Without Sog, the solution at any fixed x is found to be an increasing function of time. This feature is also observed for cases where Sog is synthesized at a slow rate or at a rate comparable to the Dpp production rate. The situation is different if the Sog production rate is significantly larger than the Dpp production rate, which is the most biologically relevant case [13]. In Figure 3, time evolution of a typical system for large $\bar{v}_S$ is plotted. It is observed that the spatial distributions of Dpp and the Dpp-receptor complex continue to have maximum concentrations at the middle of the dorsal region, $x = 0$, at any instance in time (see the left-hand panels). However, the various morphogen concentrations at $x = 0$ (the center of the dorsal region) peak at an early time, then oscillate, with the amplitude of oscillations decaying until the

concentrations reach their steady state (see the right-hand panels). Therefore we record two interesting curves for Dpp-receptor concentration: the transient solution with the largest value at the dorsal midline and the steady state solution.

In Figure 4(a), the steady state for Dpp-receptor concentration of our system (from the same numerical simulations for Figure 3) are plotted. With Sog ($\bar{v}_S \neq 0$), the Dpp-receptor in the dorsal region generally has sharper gradient and larger concentration than those without Sog ($\bar{v}_S = 0$). For the transient solution at its maximal peak magnitude, the concentration with Sog is at least double that without Sog around the middle region. These are consistent with the experimental observation in [8].

In steady state, the system with or without Sog has the same total amount of Dpp-receptor complex for $\tau = 1$. This can be shown by simply adding the right-hand sides of (11)–(13) and (13)–(14), respectively, and then integrating them through the whole domain:

$$\int_{-1}^{1} g_L \, B dx = \int_{-1}^{1} (V_L(x) - (1-\tau) V_S(x)) dx. \tag{55}$$

This relationship is independent of the presence of Sog when $\tau = 1$. In other words, the effect of inhibitor on Dpp-receptor concentration in the steady state is a spatial redistribution, not an increase or decrease in total concentration aggregated over the entire embryo if all degraded Dpp-Sog complexes, [*LS*], are cleaved to free up Dpp and degrade only the Sog component.

For the transient solution, the presence of Sog clearly helps build up the Dpp-receptor complexes in terms of both gradient and concentration, as shown in Figure 3. In Figure 4(b), we study how the transient peak of Dpp-receptor and the steady state at the dorsal midline ($x = 0$) depend on $\bar{v}_S$. The steady state for B without Sog at $x = 0$ is 0.25, and its value is plotted at the y-axis in Figure 4(b). For a small amount of Sog, the transient peaks are not high, and the steady state has the largest value at $x = 0$, as shown for $\bar{v}_S/R_0 < 0.01$. Also, $B(x = 0)$ at steady state increases as $\bar{v}_S$ increases, and the transient peak begins to deviate from the steady state around $\bar{v}_S/R_0 = 0.01$. As $\bar{v}_S$ increases by one order of magnitude from 0.015 to 0.1, the transient peak increases from 0.34 to 0.99, while the steady state only from 0.32 to 0.34. Once $\bar{v}_S/R_0$ becomes large enough, the variation of the transient peak is more sensitively dependent on variation of $\bar{v}_S/R_0$ than that of the steady state at $x = 0$. The dependence of the transient peak on other parameters such as J_{on} and J_{deg} have been investigated previously in [17] for $\tau = 1$.

When $\tau < 1$, so that only a portion of the degraded Dpp-receptor complex is cleaved to free up Dpp, the dynamics of the system strongly depends on the size of τ when the steady state condition (20)–(21) holds. It is not surprising that for smaller τ, i.e., less free Dpp released from the degraded [*LS*], the transient and steady peaks of Dpp-receptor complex are lower, as shown in Figure 5(a) for $\tau = 0.995$ and 0.99. However, for $\tau = 0.99$, the concentration of Dpp-receptor complex around the dorsal region is much lower with Sog than without Sog, as shown in Figure 5(a). As demonstrated in (55), a small change of τ will result in a large change of [*LR*] at steady state for a large $\bar{v}_S$, which is the case for Figure 5(a). In essence, $v_{eff} \equiv \bar{v}_L - (1-\tau)\,\bar{v}_S$ can be regarded as an effective production rate for Dpp.

When the effective production rate v_{eff} becomes negative, that is, the condition (20)–(21) does not hold, then the system can no longer sustain a steady state. For this situation, the concentrations of both free Dpp and the Dpp-receptor complex are typically very low, and the Dpp-receptor complex reaches the peak before Sog diffuses into the dorsal region from the ventral side and takes over the reaction with Dpp. With the availability of a large amount of Sog and its fast association rate with Dpp, Dpp-Sog reaction dominates. It is interesting to note in Figure 5(b) that as τ varies from 0.98 to 0, the time for Dpp and Dpp-receptor complex to reach their peaks barely changes. This critical time (to reach the peak) is mainly determined

by the coefficient of diffusion D_S, which controls the speed of Sog movement into the dorsal zone.

In [14] (hence also in [13]), degradation for [*LR*] is not allowed in the system ($K_{deg} = 0$); therefore the condition (20)–(21) does not hold for any $\bar{v}_L > 0$. In order to achieve steady state in [13], [14], the models there turned off production of Dpp after 10 minutes ($T^* = 10$ minutes). The effect of the choice of T^* and the biological background for the choice $T^* = 10$ minutes were not discussed in [13] and [14]. In Figure 6, we study how our system reacts to the choice of T^* if $K_{deg} = 0$. It is found that the evolution of [*LR*] at the dorsal midline becomes monotone, unlike the case in Figure 3, and as expected, the time to reach steady states strongly depends on the choice of T^*. In Figure 6, the steady states for [*LR*] are shown for $T^* = 5, 8, 10, 12, 15, 20, 30, 45, 60$ minutes. The concentration of [*LR*] varies almost linearly with respect to T^* until the receptors are close to being fully occupied when T^* is large.

Finally, we investigate the effect of diffusion. In Figure 7, Dpp-receptor complexes as functions of time and space are shown for five different choices of diffusion constants. Case (a) has all three diffusion constants the same as in Figure 3, cases (b)–(d) have one of the diffusion constants being 1% of the corresponding value in case (a), and the case (e) has two constants at 1% of the corresponding values in case (a). Similarly in Figure 8, some of the diffusion constants are 10-fold larger than others.

As shown in case (b) of both Figures 7 and 8, the magnitude of the diffusion co-efficient for Dpp has very little effect on the broadness and intensity of Dpp activity at the dorsal midline. This is consistent with the behavior of the leading term perturbation solution. A larger diffusion for Dpp reduces the peak of transient Dpp-activity at the midline slightly and broadens it slightly. On the other hand, a decrease in diffusion constant for Dpp-Sog complexes, as in cases (d) and (e), significantly broadens the Dpp activity around the midline for both peak transient and steady state distributions, with the height of only the transient peak reduced significantly but with almost the same steady state at $x = 0$. The time to steady state and transient peaks seems to be insensitive to the change of the diffusion constants for Dpp or the Dpp-Sog complex.

As predicted by the perturbation solutions, varying the diffusion coefficient for Sog changes the Dpp activity around the dorsal midline significantly. As shown in Figure 7(c), a smaller diffusion of Sog relative to the diffusion of Dpp leads to more concentrated transient Dpp activity around the dorsal midline, but it takes much longer to reach the steady state, with a monotone increase of Dpp activity around the dorsal midline (i.e., there is no transient peak). On the other hand, larger diffusion of Sog relative to the diffusion of Dpp weakens and broadens the Dpp activity, as in Figure 8(c).

6. Conclusions

The dynamics of Dpp activities in the presence of the inhibitor Sog is analyzed herein to initiate a study of dorsal-ventral morphogen gradient formation in vertebrates and *Drosophila* embryos. Here we investigate a prototype morphogen system with typical ligand diffusion and degradation, but now with the additional feature of cleavage of Dpp-Sog complexes by Tolloid to free up Dpp. Among the principal results of our investigation is the establishment of a simple and biologically meaningful necessary and sufficient condition for the existence of a steady state gradient in the system. This condition requires a balance of the production rates of ligands, degradation rate of ligand-receptor complex, and rate of cleavage of ligand-inhibitor complex. For high Sog production rates (relative to the Dpp production rate), a perturbation solution has been obtained in terms of elementary functions. This solution exhibits an intense Dpp-receptor concentration near the dorsal midline. Numerical simulations of the *evolution* of the system

confirmed these features of the steady state behavior. In addition, a transient peak of Dpp-receptor concentration at the dorsal midline was found to be even more intense prior to steady state, reaching more than twice the level of the steady state at its peak amount. This transient peak is more sensitively dependent on variation of the production of Sog than the steady state peak. The high Dpp-receptor concentration around the dorsal midline and other features of the system are consistent with experimental observations.

Acknowledgements

The authors acknowledge the very helpful discussions with A. Lander and L. Marsh. Part of this work was done when Y. L. was visiting the Department of Mathematics of UCI, and he would like to express appreciation for the hospitality he received.

References

1. Wolpert, L.; Beddington, R.; Brockes, J.; Jessel, T.; Lawrence, P.; Meyerowitz, E. Principles of Development. 2. Oxford University Press; Oxford, UK: 2002.
2. Teleman AA, Strigini M, Cohen SM. Shaping morphogen gradients. Cell 2001;105:559–562. [PubMed: 11389824]
3. Gurdon JB, Bourillot PY. Morphogen gradient interpretation. Nature 2001;413:797–803. [PubMed: 11677596]
4. Lander A, Nie Q, Wan FYM. Do morphogen gradients arise by diffusion? Dev Cell 2002;2:785–796. [PubMed: 12062090]
5. Bier E. A unity of opposites. Nature 1999;398:375–376. [PubMed: 10201364]
6. Ashe HL, Levine M. Local inhibition and long-range enhancement of Dpp signal transduction by Sog. Nature 1999;398:427–431. [PubMed: 10201373]
7. Oelgeschlager M, Larrain J, Geissert D, Robertis EM. The evolutionarily conserved BMP-binding protein twisted gastrulation promotes BMP signalling. Nature 2000;405:757–762. [PubMed: 10866189]
8. Ross J, Shimmi O, Vilmos P, Petryk A, Kim H, Gaudenez K, Hermanson S, Ekker A, O'Connor M, Marsh JL. Twisted gastrulation is a conserved extracellular BMP antagonist. Nature 2001;410:479–483. [PubMed: 11260716]
9. Lou Y, Nie Q, Wan FYM. Nonlinear eigenvalue problems in the stability analysis of morphogen gradients. Stud Appl Math 2004;113:183–215.
10. Lander A, Nie Q, Vargas B, Wan FYM. Aggregation of a distributed source in morphogen gradient formation. Stud Appl Math. 2005to appear.
11. Lander A, Nie Q, Wan FYM. Spatially distributed morphogen production and morphogen gradient formation. Math Biosci Eng. 2005to appear.
12. Lander A, Nie Q, Wan FYM. Internalization and end flux in morphogen gradient formation. J Comput Appl Math. 2005to appear.
13. Eldar A, Dorfman R, Weiss D, Ashe H, Shilo B, Barkai N. Robustness of the BMP morphogen gradient in *Drosophila* embryonic patterning. Nature 2002;419:304–308. [PubMed: 12239569]
14. Eldar A, Dorfman R, Weiss D, Ashe H, Shilo B, Barkai N. Supplement—Robustness of the BMP morphogen gradient in *Drosophila* embryonic patterning. Nature 2002;419:304–308. [PubMed: 12239569]
15. Eldar A, Rosin D, Shilo BZ, Barkai N. Self-enhanced ligand degradation underlies robustness of morphogen gradients. Dev Cell 2003;5:635–646. [PubMed: 14536064]
16. Wang Z, Marcu O, Berns MW, Marsh JL. In vivo FCS measurements of ligand diffusion in intact tissues. Proc SPIE 2004;5323:177–183.
17. Kao, J.; Nie, Q.; Teng, A.; Wan, FYM.; Lander, A.; Marsh, IL. Proceeding of the 2nd MIT Conference on Computational Mechanics. 2. Elsevier Press; New York: 2003. Can morphogen activity be enhanced by its inhibitors?; p. 1729-1734.
18. Mizutani C, Nie Q, Wan FYM, Zhang Y, Vilmos P, Bier E, Marsh L, Lander A. Origin of the BMP activity gradient in the *Drosophila* embryo. Devel Cell. 2005to appear.

19. Crick FC. Diffusion in embryogenesis. Nature 1970;225:40–42.
20. Kerszberg M, Wolpert L. Mechanisms for positional signalling by morphogen transport: A theoretical study. J Theoret Biol 1998;191:103–114. [PubMed: 9593661]
21. Piccolo S, Agiusa E, Lu B, Goodman S, Dale L, De Robertis E. Cleavage of chordin by Xolloid metalloprotease suggests a role for proteolytic processing in the regulation of Spemann organizer activity. Cell 1997;91:407–416. [PubMed: 9363949]
22. Marques G, Musacchio M, Shimell MJ, Stapleton KW, Cho K, O'Connor M. Production of a Dpp activity gradient in the early Drosophila embryo through the opposing actions of the Sog and TLD proteins. Cell 1997;91:417–426. [PubMed: 9363950]
23. Protter, MH.; Weinberger, HF. Maximum Principle in Differential Equations. 2. Springer-Verlag; Berlin: 1984.
24. Smoller, J. Shock Waves and Reaction-Diffusion Equations. 2. Springer-Verlag; New York: 1994.
25. Strikwerda, JC. Finite Difference Schemes and Partial Differential Equations. Wadsworth & Brooks/Cole Advanced Books & Software; Pacific Grove, CA: 1989.

Appendix A

Proof of Lemma 3.4

We show that there exists $M_1 > 0$ such that $\|\tilde{C}\|L^\infty \le M_1$. As in the proof of Lemma 3.3, $\|C\|L^1 \le M_2$ for some constant $M_2 > 0$. Integrating (27) in (−1, 1), we get

$$\int_{-1}^{1} h_{LS}\tilde{A}\tilde{D} = \int_{-1}^{1} (f_{LS} + g_{LS})\tilde{C}, \tag{56}$$

which implies that $\int_{-1}^{1}\tilde{A}\tilde{D} \le M_3\int_{-1}^{1}\tilde{C} \le M_2M_3$ for some $M_3 > 0$. Integrating (27) from −1 to x, we get

$$\rho_{LS}\tilde{C}_{,x} + \lambda\int_{-1}^{x}[h_{LS}\tilde{A}\tilde{D} - (f_{LS} + g_{LS})\tilde{C}] = 0, \quad -1 < x < 1. \tag{57}$$

Hence

$$\rho_{LS}\|\tilde{C}_{,x}\|_{L^\infty} \le \|h_{LS}\|_{L^\infty}\int_{-1}^{1}\tilde{A}\tilde{D} + \|f_{LS} + g_{LS}\|_{L^\infty}\int_{-1}^{1}\tilde{C} \le M_4 \tag{58}$$

for some constant $M_4 > 0$. This along with $\int_{-1}^{1}\tilde{C} \le M_2$ implies the L^∞ bound of $\tilde{C}$, which is independent of λ.

Next we show that there exists some constant $M_5 > 0$ such that $\|\tilde{A}\|L^\infty \le M_5$. To this end, adding up (26) and (27) and integrating from −1 to x, we get

$$\rho_L\tilde{A}_{,x} + \rho_{LS}\tilde{C}_{,x} = \lambda\int_{-1}^{x}\left[\frac{g_L h_L\tilde{A}}{f_L + g_L + h_L\tilde{A}} + (1-\tau)g_{LS}\tilde{C} - V_L\right], \tag{59}$$

which implies that

$$\|\tilde{A}_{,x}\|_{L^\infty} \le M_6\left(\|\tilde{C}_{,x}\|_{L^\infty} + \|g_L\|_{L^\infty} + \|\rho_{LS}\|_{L^\infty}\int_{-1}^{1}\tilde{C} + \|V_L\|_{L^\infty}\right) := M_7. \tag{60}$$

We claim that there exists some constant $M_8 > 0$ such that $\int_{-1}^{1} \tilde{A} \le M_8$. To establish this assertion, we argue by contradiction: if not, passing to a subsequence if necessary, we may assume that $\int_{-1}^{1} \tilde{A} \to +\infty$. This together with (60) implies that

$$\left| \frac{\tilde{A}(x)}{\int_{-1}^{1} \tilde{A}} - 1 \right| \le \frac{\| \tilde{A}_{,x} \|_{L^\infty}}{\int_{-1}^{1} \tilde{A}} \le \frac{M_7}{\int_{-1}^{1} \tilde{A}} \to 0 \quad \forall \ -1 \le x \le 1. \tag{61}$$

Hence $\tilde{A} \to +\infty$ uniformly. Similar to (24) we have

$$\int_{-1}^{1} V_L = \int_{-1}^{1} \frac{g_L h_L \tilde{A}}{f_L + g_L + h_L \tilde{A}} + (1 - \tau) \int_{-1}^{1} V_S. \tag{62}$$

By (61) we have $\int_{-1}^{1} \frac{g_L h_L \tilde{A}}{f_L + g_L + h_L \tilde{A}} \to \int_{-1}^{1} g_L$, which together with (62) implies that $\int_{-1}^{1} V_L = \int_{-1}^{1} g_L + (1 - \tau) \int_{-1}^{1} V_S$. However, this contradicts (21). Therefore $\int_{-1}^{1} \tilde{A}$ is uniformly bounded for $\lambda \in (0, 1]$. This together with (60) yields $\|\tilde{A}\|_{L^\infty} \le M_5$ for some $M_5 > 0$.

Finally we show that there exists some constant $M_9 > 0$ such that $\|\tilde{D}\|_{L^\infty} \le M_9$. We argue by contradiction: suppose not; passing to a subsequence if necessary, we may assume that $\|\tilde{D}\|_{L^\infty} \to \infty$ and $\lambda \to \hat{\lambda} \in [0, 1]$. Set $\hat{D}(x) = \frac{\tilde{D}(x)}{\| \tilde{D} \|_{L^\infty}}$. Then $\hat{D}$ satisfies $\hat{D}_{,x}(-1) = \hat{D}_{,x}(1) = 0$, $\|\hat{D}\|_{L^\infty} = 1$, and

$$\rho_{LS} \hat{D}_{,xx} + \lambda \left[- h_{LS} \tilde{A} \hat{D} + \frac{f'_{LS} \tilde{C} + V_S}{\| \tilde{D} \|_{L^\infty}} \right] = 0, \quad -1 < x < 1. \tag{63}$$

Since $\|\tilde{A}\|_{L^\infty}$, $\|\tilde{A}_{,x}\|_{L^\infty}$ are uniformly bounded, we may assume that $\tilde{A}(x) \to A^*(x)$ uniformly in $[-1, 1]$. From (62) and (20) we see $\int_{-1}^{1} \tilde{A} \ge M_{10} > 0$ for some constant M_{10}. Hence $A^* \not\equiv 0$ since $\int_{-1}^{1} A^* \ge M_{10} > 0$. By standard regularity theory we may assume that $\hat{D}(x) \to D^*(x)$ in $C^1[-1, 1]$, and D^* is a weak solution of

$$\rho_{LS} D^*_{,xx} - \hat{\lambda} h_{LS} A^* D^* = 0, \quad -1 < x < 1, \quad D^*_{,x}(-1) = D^*_{,x}(1) = 0. \tag{64}$$

Moreover, $D^* \ge 0$ in $[-1, 1]$ and $\|D^*\|_{L^\infty} = 1$. If $\hat{\lambda} > 0$, since $A^* \not\equiv 0$, $A^* \ge 0$, by the maximum principle we see that $D^* \equiv 0$, which contradicts $\|D^*\|_{L^\infty} = 1$; if $\hat{\lambda} = 0$, then it follows from (64) that $D^* \equiv 1$, i.e., $\hat{D}(x) \to 1$ uniformly. Dividing (56) by $\|D\|_{L^\infty}$, we have $\int_{-1}^{1} h_{LS} \tilde{A} \hat{D} = \int_{-1}^{1} (f_{LS} + g_{LS}) \tilde{C} / \| \tilde{D} \|_{L^\infty}$. Then we obtain $\int_{-1}^{1} h_{LS} A^* = 0$, which implies that $A^* \equiv 0$. Contradiction! This completes the proof of (34).

When $\lambda = 0$, $(\tilde{A}, \tilde{C}, \tilde{D})$ is a solution of (26)–(29) if and only if $\tilde{A}$, $\tilde{C}$, and $\tilde{D}$ are all constants. It turns out that a particular triple, denoted by $(\hat{A}, \hat{C}, \hat{D})$, is special, where $\hat{A}$, $\hat{C}$, $\hat{D}$ are defined as follows: by (20)–(21) it is easy to see that there is a unique positive constant, denoted by $\hat{A}$, such that

$$\int_{-1}^{1} \frac{g_L h_L \hat{A}}{f_L + g_L + h_L \hat{A}} = \int_{-1}^{1} V_L - (1 - \tau) \int_{-1}^{1} V_S. \tag{65}$$

Set

$$\hat{D} = \frac{\int_{-1}^{1}(f_{LS} + g_{LS})\int_{-1}^{1} V_S}{\hat{A}\int_{-1}^{1} h_{LS}\int_{-1}^{1} g_{LS}}, \quad \hat{C} = \frac{\int_{-1}^{1} V_S}{\int_{-1}^{1} g_{LS}}. \tag{66}$$

Lemma A.1

Suppose that (20)–(21) *holds. Let* $(A_\lambda, B_\lambda, C_\lambda)$ *denote positive solutions of* (26)–(29). *Then as* $\lambda \to 0+$, $(A_\lambda, B_\lambda, C_\lambda) \to (\hat{A}, \hat{C}, \hat{D})$ *uniformly.*

Proof

By Lemma 3.4, $(A_\lambda, B_\lambda, C_\lambda)$ are uniformly bounded. By standard regularity theory and the embedding theorem, passing to a subsequence if necessary, we may assume that $(A_\lambda, B_\lambda, C_\lambda) \to (\hat{A}, \hat{C}, \hat{D})$ uniformly, where $\bar{A}$, $\bar{C}$, and $\bar{D}$ satisfy $\bar{A}_{xx} = \bar{C}_{xx} = \bar{D}_{xx} = 0$, and $\bar{A}_x = \bar{C}_x = \bar{D}_x = 0$ at $x = -1, 1$. Therefore $\bar{A}$, $\bar{C}$, $\bar{D}$ are all nonnegative constants. Passing to the limit in (62) (with $\tilde{A}$ being replaced by A_λ), we have $\bar{A} = \hat{A}$. Similarly we can show that $\hat{C} = \bar{C}$ and $\hat{D} = \bar{D}$. Since the limit $(\hat{A}, \hat{C}, \hat{D})$ is unique, the convergence $(A_\lambda, B_\lambda, C_\lambda) \to (\hat{A}, \hat{C}, \hat{D})$ is true for the whole sequence, and the limit is uniform in x.

Lemma A.2

There exists some constant $\delta_1 > 0$ *such that if* $0 < \lambda \le \delta_1$, (26)–(29) *has a unique positive solution.*

Proof

Set $X = \{u \in C[-1, 1] : \int_{-1}^{1} u(x)dx = 0\}$, $Z = \{u \in X : u_{,x}(-1) = u_{,x}(1) = 0\}$, and define the projection operator $P : C[-1, 1] \to X$ by $Pu = u - \int_{-1}^{1} u(x)dx$. For $(\lambda, A_0, a_0, C_0, c_0, D_0, d_0) \in R^1 \times (Z \times R^1)^3$, define $F : R^1 \times (Z \times R^1)^3 \to (X \times R^1)^3$ by

$$F(\lambda, A_0, a_0, C_0, c_0, D_0, d_0) = \begin{pmatrix} \rho_L A_{0,xx} + \lambda P F_1^+(x, A_0 + a_0, C_0 + c_0, D_0 + d_0) \\ \int_{-1}^{1} F_1^+(x, A_0 + a_0, C_0 + c_0, D_0 + d_0)dx \\ \rho_{LS} C_{0,xx} + \lambda P F_2(x, A_0 + a_0, C_0 + c_0, D_0 + d_0) \\ \int_{-1}^{1} F_2(x, A_0 + a_0, C_0 + c_0, D_0 + d_0)dx \\ \rho_S D_{0,xx} + \lambda P F_3(x, A_0 + a_0, C_0 + c_0, D_0 + d_0) \\ \int_{-1}^{1} F_3(x, A_0 + a_0, C_0 + c_0, D_0 + d_0)dx \end{pmatrix} \tag{67}$$

By the definition of $\hat{A}$, $\hat{C}$, $\hat{D}$, $F(0, \hat{A}, \hat{C}, \hat{D}, 0, 0, 0) = (0, 0, 0, 0, 0, 0)$. The Fréchet derivative of F with respect to $(A_0, a_0, C_0, c_0, D_0, d_0)$ at $(\lambda, A_0, a_0, C_0, c_0, D_0, d_0) = (0, \hat{A}, 0, \hat{C}, 0, \hat{D}, 0)$ is given by

$$D_{(A_0,a_0,C_0,c_0,D_0,d_0)}F|_{(0,\hat{A},0,\hat{C},0,\hat{D},0)} = \begin{pmatrix} \rho_L \frac{d^2}{dx^2} & 0 & 0 & 0 & 0 & 0 \\ 0 & \rho_{LS}\frac{d^2}{dx^2} & 0 & 0 & 0 & 0 \\ 0 & 0 & \rho_S\frac{d^2}{dx^2} & 0 & 0 & 0 \\ * & * & * & & & \\ * & * & * & M_{3\times 3} & & \\ * & * & * & & & \end{pmatrix}, \tag{68}$$

where $M_{3\times 3}$ is the 3 × 3 matrix

$$\begin{pmatrix} \int_{-1}^{1}\left[\frac{-g_L h_L (f_L+g_L)}{(f_L+g_L+h_L\hat{A})^2} - h_{LS}\hat{D}\right] & \int_{-1}^{1}(f_{LS}+\tau g_{LS}) & -(\int_{-1}^{1}h_{LS})\hat{A} \\ (\int_{-1}^{1}h_{LS})\hat{D} & -\int_{-1}^{1}(f_{LS}+g_{LS}) & (\int_{-1}^{1}h_{LS})\hat{A} \\ -(\int_{-1}^{1}h_{LS})\hat{D} & \int_{-1}^{1}f_{LS} & -(\int_{-1}^{1}h_{LS})\hat{A} \end{pmatrix}. \tag{69}$$

Since the operator $\frac{d^2}{dx^2}$, subject to the no flux boundary condition, is an isomorphism from Z to X, we see that the operator $D_{(A_0,a_0,C_0,c_0,D_0,d_0)}F|_{(0,\hat{A},0,\hat{C},0,D,0)}$ is invertible from $(Z \times R^1)^3$ to $(X \times R^1)^3$ if and only if the matrix $M_{3\times 3}$ is invertible. It is straightforward to check that the determinant of $M_{3\times 3}$ is equal to

$$\left(\int_{-1}^{1}h_{LS}\right)\hat{D}\cdot\int_{-1}^{1}(f_{LS}+g_{LS})\cdot\left(\int_{-1}^{1}h_{LS}\right)\hat{A}(1-\gamma_2)(-\gamma_1), \tag{70}$$

where γ_1, γ_2 are defined as

$$\gamma_1 = \frac{\int_{-1}^{1}\frac{g_L h_L (f_L+g_L)}{(f_L+g_L+h_L\hat{A})^2}}{\left(\int_{-1}^{1}h_{LS}\right)\hat{D}}, \quad \gamma_2 = \frac{\int_{-1}^{1}f_{LS}}{\int_{-1}^{1}(f_{LS}+g_{LS})}. \tag{71}$$

Since $\gamma_1 > 0$ and $0 < \gamma_2 < 1$, $M_{3\times 3}$ is nondegenerate.

By the implicit function theorem, there exists $\delta_2 > 0$ such that if $0 < \lambda = \delta_2$, there is a unique solution to $F = 0$, denoted by $(A_\lambda(x), a_\lambda(x), C_\lambda(x), c_\lambda(x), D_\lambda(x), d_\lambda(x))$, in some neighborhood of $(\hat{A}, 0, \hat{C}, 0, \hat{D}, 0)$. As $\lambda \to 0+$, $(A_\lambda, a_\lambda, C_\lambda, c_\lambda, D_\lambda, d_\lambda) \to (\hat{A}, 0, \hat{C}, 0, D, 0)$ uniformly. In particular, for $0 < \leq = \delta_2$, $(A_\lambda+a_\lambda, C_\lambda+c_\lambda, D_\lambda+d_\lambda)$ is the unique positive solution of (26)–(29) in some neighborhood of $(\hat{A}, \hat{C}, D)$. This and Lemma A.1 imply that, for $0 < \lambda \ll 1$, (26)–(29) has a unique positive solution.

Lemma A.3

Let (A^*, C^*, D^*) *denote the unique positive solution of* (26)–(29) *for* $0 < \lambda \ll 1$. *Then for* $0 < \lambda \ll 1$, *the Fréchet derivative of* $T(\lambda)$ *with respect to* $(\tilde{A}, C, D)$ *at* (A^*, C^*, D^*), *denoted by* $D_{(\tilde{A},\tilde{C},\tilde{D})}T(\lambda)\,|_{(A^*,C^*,D^*)}$, *has no eigenvalue greater than or equal to* 1.

Proof

By (35), $D_{(\tilde{A},\,\tilde{C},\,\tilde{D})}T(\lambda)|_{(A^*,C^*,D^*)}(\phi_1,\,\phi_2,\,\phi_3)$ is given by

$$\begin{pmatrix} L_{\rho_L}^{-1}\left\{\left[1+\lambda\frac{\partial F_1}{\partial A}(x,\,A^*,\,C^*,\,D^*)\right]\phi_1+\lambda\frac{\partial F_1}{\partial C}\phi_2+\lambda\frac{\partial F_1}{\partial D}\phi_3\right\} \\ L_{\rho_{LS}}^{-1}\left\{\lambda\frac{\partial F_2}{\partial A}\phi_1+\left[1+\lambda\frac{\partial F_2}{\partial C}\right]\phi_2+\lambda\frac{\partial F_2}{\partial D}\phi_3\right\} \\ L_{\rho_S}^{-1}\left\{\lambda\frac{\partial F_3}{\partial A}\phi_1+\lambda\frac{\partial F_3}{\partial C}\phi_2+\left[\lambda\frac{\partial F_3}{\partial D}+1\right]\phi_3\right\} \end{pmatrix},$$

where $\frac{\partial F_i}{\partial A}$, $\frac{\partial F_i}{\partial C}$, $\frac{\partial F_i}{\partial D}$ (i = 1, 2, 3) are evaluated at (x, A^*, C^*, D^*).

We argue by contradiction: suppose that Lemma A.3 fails. Passing to a subsequence if necessary, we may assume that for $0<\lambda\ll 1$ the operator $D_{(\tilde{A},\,\tilde{C},\,\tilde{D})}T(\lambda)|_{(A^*,C^*,D^*)}$ has eigenvalue $\mu=\mu(\lambda)\geq 1$, with the corresponding eigenfunction $(\phi_1,\,\phi_2,\,\phi_3)$ normalized by $\|\phi_1\|L^\infty+\|\phi_2\|L^\infty+\|\phi_3\|L^\infty=1$. Then $(\phi_1,\,\phi_2,\,\phi_3)$ satisfies

$$-\mu\rho_L\frac{d^2\phi_1}{dx^2}+(\mu-1)\phi_1=\lambda\left[\frac{\partial F_1}{\partial A}\phi_1+\frac{\partial F_1}{\partial C}\phi_2+\frac{\partial F_1}{\partial D}\phi_3\right], \tag{72}$$

$$-\mu\rho_{LS}\frac{d^2\phi_2}{dx^2}+(\mu-1)\phi_2=\lambda\left[\frac{\partial F_2}{\partial A}\phi_1+\frac{\partial F_2}{\partial C}\phi_2+\frac{\partial F_2}{\partial D}\phi_3\right], \tag{73}$$

$$-\mu\rho_S\frac{d^2\phi_3}{dx^2}+(\mu-1)\phi_3=\lambda\left[\frac{\partial F_3}{\partial A}\phi_1+\frac{\partial F_3}{\partial C}\phi_2+\frac{\partial F_3}{\partial D}\phi_3\right], \tag{74}$$

$$(\phi_1)_{,x}=(\phi_2)_{,x}=(\phi_3)_{,x}=0 \text{ at } x=-1,\,1, \tag{75}$$

where $\frac{\partial F_i}{\partial A}$, $\frac{\partial F_i}{\partial C}$, $\frac{\partial F_i}{\partial D}$ (i = 1, 2, 3) in (72)–(74) are evaluated at $(\tilde{A},\,\tilde{C},\,\tilde{D})=(A^*,\,C^*,\,D^*)$.

It is easy to see that $\mu(\lambda)\to 1$ as $\lambda\to 0+$, and the corresponding eigenfunctions $(\phi_1,\,\phi_2,\,\phi_3)\to(\phi_1,\,\phi_2,\,\phi_3)$ uniformly, where $(\phi_1,\,\phi_2,\,\phi_3)$ are constants satisfying $|\phi_1|+|\phi_2|+|\phi_3|=1$. Set $\mu(\lambda)=1+\lambda\mu_1(\lambda)$. Since $\mu(\lambda)\geq 1$, we have $\mu_1(\lambda)\geq 0$. Integrating (72)–(74), we get

$$\int_{-1}^{1}\left[\frac{\partial F_1}{\partial A}-\mu_1\right]\phi_1+\int_{-1}^{1}\frac{\partial F_1}{\partial C}\phi_2+\int_{-1}^{1}\frac{\partial F_1}{\partial D}\phi_3=0, \tag{76}$$

$$\int_{-1}^{1}\frac{\partial F_2}{\partial A}\phi_1+\int_{-1}^{1}\left[\frac{\partial F_2}{\partial C}-\mu_1\right]\phi_2+\int_{-1}^{1}\frac{\partial F_2}{\partial D}\phi_3=0, \tag{77}$$

$$\int_{-1}^{1}\frac{\partial F_3}{\partial A}\phi_1+\int_{-1}^{1}\frac{\partial F_3}{\partial C}\phi_2+\int_{-1}^{1}\left[\frac{\partial F_3}{\partial D}-\mu_1\right]\phi_3=0. \tag{78}$$

We first prove that $\mu_1(\lambda)$ is uniformly bounded for all $0<\lambda\ll 1$. If not, passing to a subsequence if necessary, we may assume that as $\lambda\to 0+$, $\mu_1(\lambda)\to+\infty$. Divide (76) by μ_1; passing to the limit, we find that $\phi_1=0$. Similarly, $\phi_2=\phi_3=0$. However, this contradicts $|\phi_1|+|\phi_2|+|\phi_3|=1$. Therefore $\mu_1(\lambda)$ is nonnegative and uniformly bounded. Passing to a subsequence if necessary, we may assume that $\mu_1(\lambda)\to\bar{\mu_1}\geq 0$ as $\lambda\to 0+$.

Passing to the limit in (76)–(78), by Lemma A.1, $(M_{3\times3} - \bar{\mu_1} I_{3\times3})(\phi_1, \phi_2, \phi_3) = (0, 0, 0)$. Since $(\phi_1, \phi_2, \phi_3) \neq (0, 0, 0)$, $|M_{3\times3} - \bar{\mu_1} I_{3\times3}| = 0$. However, direct calculation yields that $|M_{3\times3} - \bar{\mu_1} I_{3\times3}|$ is equal to

$$
\begin{aligned}
&-\left(\int_{-1}^{1} h_{LS}\right)\hat{D}\cdot\int_{0}^{1}(f_{LS}+g_{LS})\cdot\left(\int_{-1}^{1} h_{LS}\right)\hat{A}\\
&\cdot\left\{\left(\gamma_1+\frac{\mu_1}{(\int_{-1}^{1} h_{LS})\hat{D}}\right)\cdot\left(1+\frac{\mu_1}{\int_{-1}^{1}(f_{LS}+g_{LS})}\right)\cdot\frac{\mu_1}{(\int_{-1}^{1} h_{LS})\hat{A}}\right.\\
&+\left[(1-\tau)(1-\gamma_2)+\frac{\mu_1}{\int_{-1}^{1}(f_{LS}+g_{LS})}\right]\cdot\frac{\mu_1}{\int_{-1}^{1} h_{LS}\hat{A}}\\
&\left.+\left(\gamma_1+\frac{\mu_1}{(\int_{-1}^{1} h_{LS})\hat{D}}\right)\cdot\left(1-\gamma_2+\frac{\mu_1}{\int_{-1}^{1}(f_{LS}+g_{LS})}\right)\right\},
\end{aligned}
$$

which is negative since $\bar{\mu_1} \geq 0$, $\gamma_1 > 0$, $0 \leq \tau \leq 1$, and $\gamma_2 < 1$. Contradiction! This completes the proof of Lemma A.3.

Proof of Proposition 3.5

By Lemma A.2, for $0 < \lambda \ll 1$, $T(\lambda)$ has a unique fixed point. By Lemma A.3, 1 is not an eigenvalue of $D_{(\tilde{A}, \tilde{C}, \tilde{D})} T(\lambda)|_{(A^*, C^*, D^*)}$. Hence deg $(I - T(\lambda), \Omega, (0, 0, 0) = (-1)^{\beta}$, where β is the number of eigenvalues (counting algebraic multiplicity) of $D_{(\tilde{A}, \tilde{C}, \tilde{D})} T(\lambda)|_{(A^*, C^*, D^*)}$, which is greater than 1. By Lemma A.3 we see that $\beta = 0$. Hence deg $(I - T(\lambda), \Omega, (0, 0, 0) = 1$ for $0 < \lambda \ll 1$.

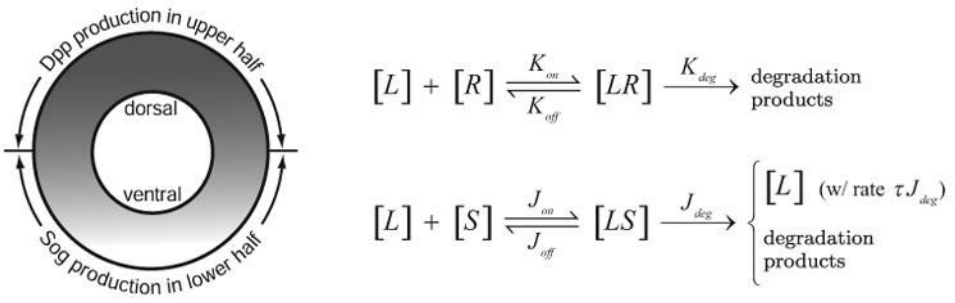

Fig. 1.
Cross section of a Drosophila embryo, and the reaction schemes with rate constants.

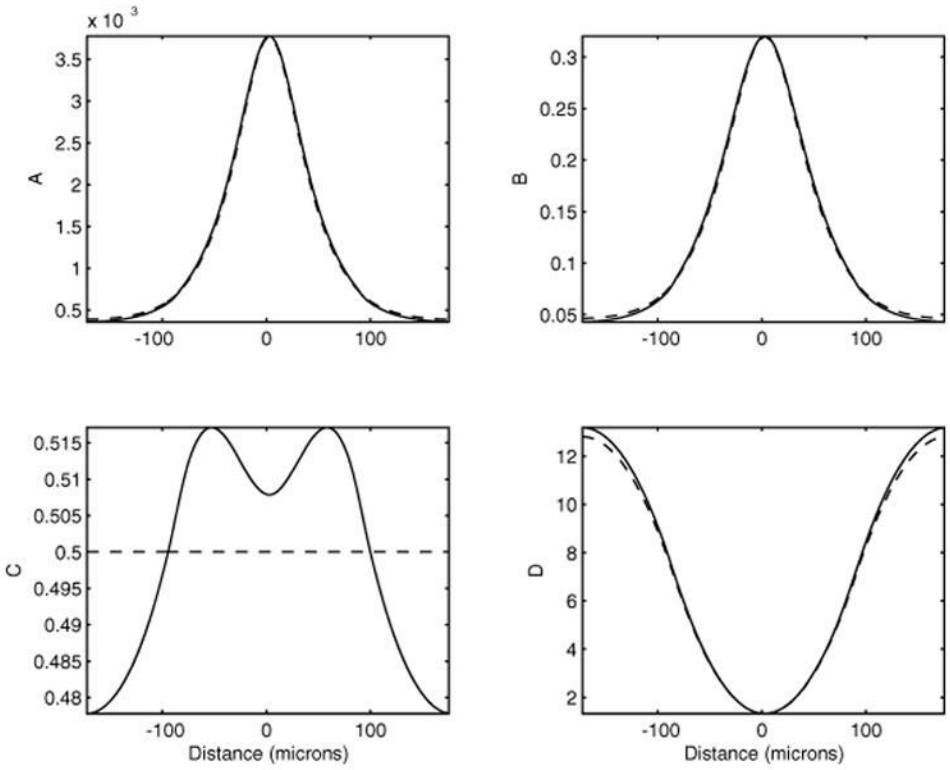

Fig. 2.

Comparisons between the numerical steady states (solid lines) and the perturbation solutions (dashed lines). The parameters are $\bar{v}_L = 8 \times 10^{-4} s^{-1} \mu M$, $K_{on} = 0.4 s^{-1}$, $K_{off} = 4 \times 10^{-6} s^{-1}$, $K_{deg} = 3.2 \times 10^{-3}\ s^{-1}$, $\bar{v}_S = = 6 \times 10^{-2}\ s^{-1} \mu M$, $J_{on} = 6 s^{-1} \mu M$, $J_{off} = 10^{-5} s^{-1}$, $J_{deg} = 6 \times 10^{-2} s^{-1}$, $\tau = 1$.

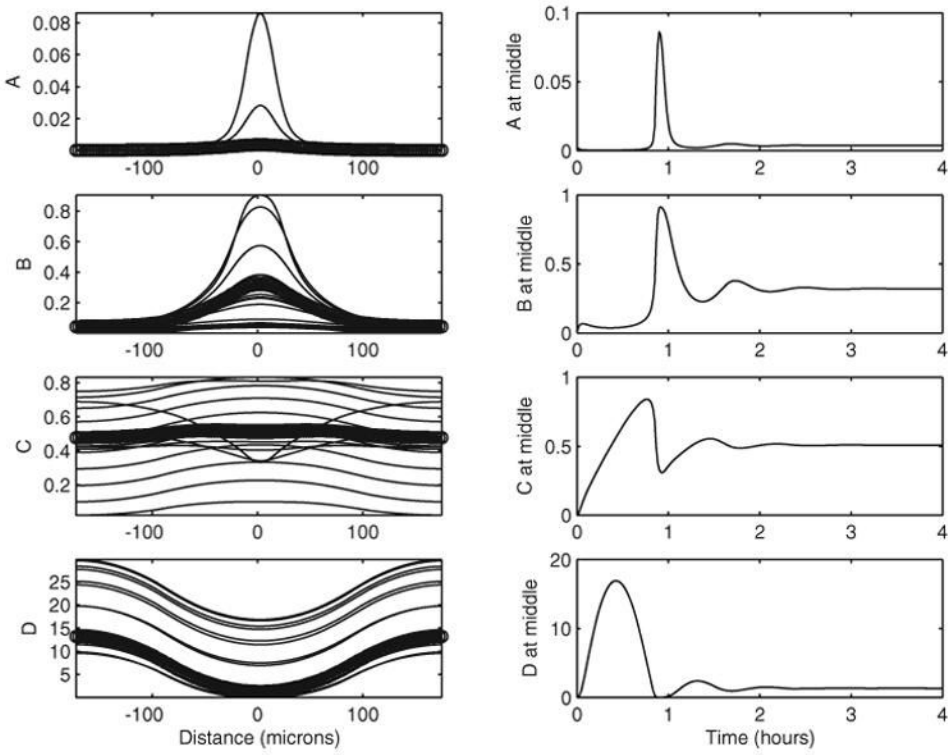

Fig. 3.

The dynamics of solutions with SOG at every 5 minutes; o in the left-hand panels marks the steady-state solutions. All parameters are the same as for Figure 2.

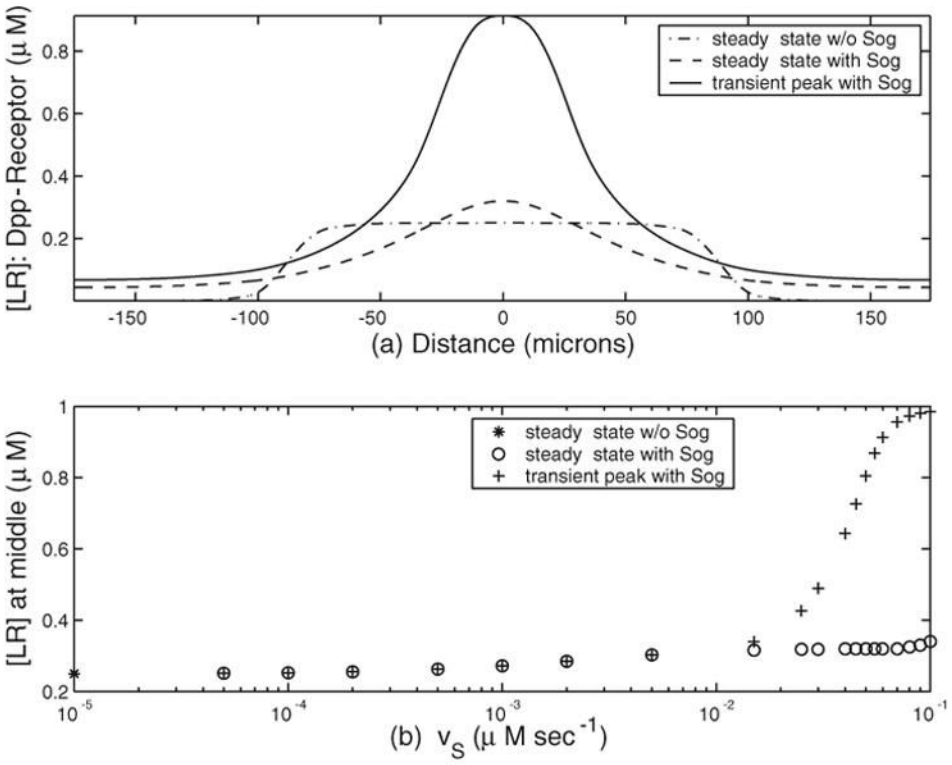

Fig. 4.

Effect of Sog on the transient and steady state solutions. (a) [LR] as a function of space; (b) [LR] at dorsal midline as a function of $\bar{v}_S$. Parameters are as in Figure 3.

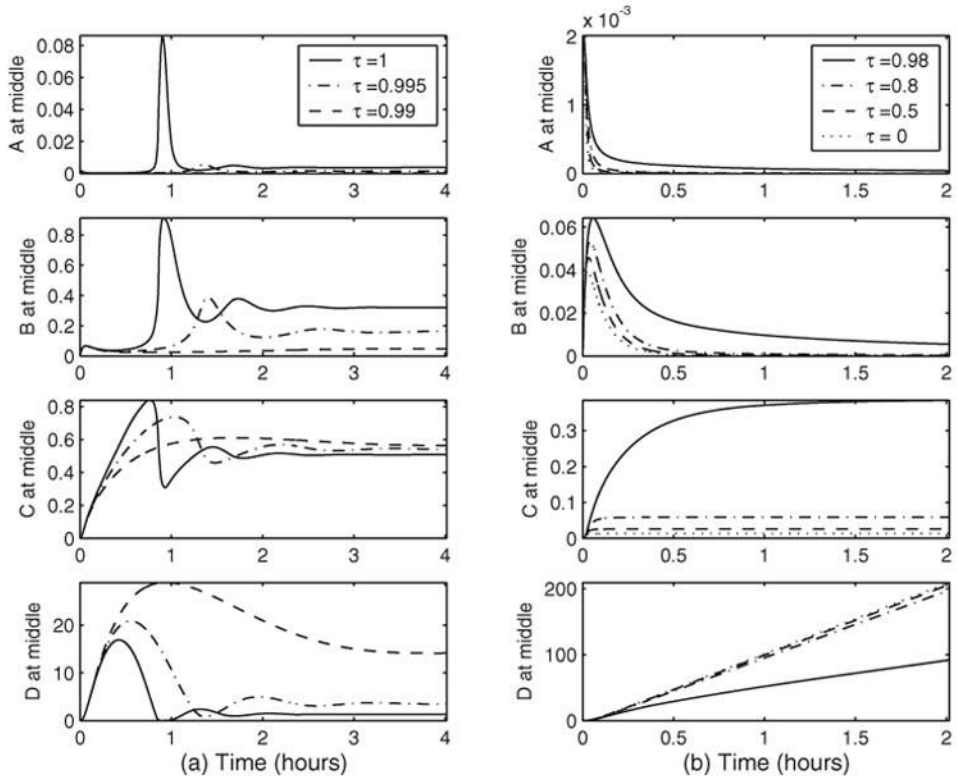

Fig. 5.

Effect of τ on the steady state solutions. Parameters are as in Figure 3 except for τ. (a) Cases with steady states; (b) cases without steady states.

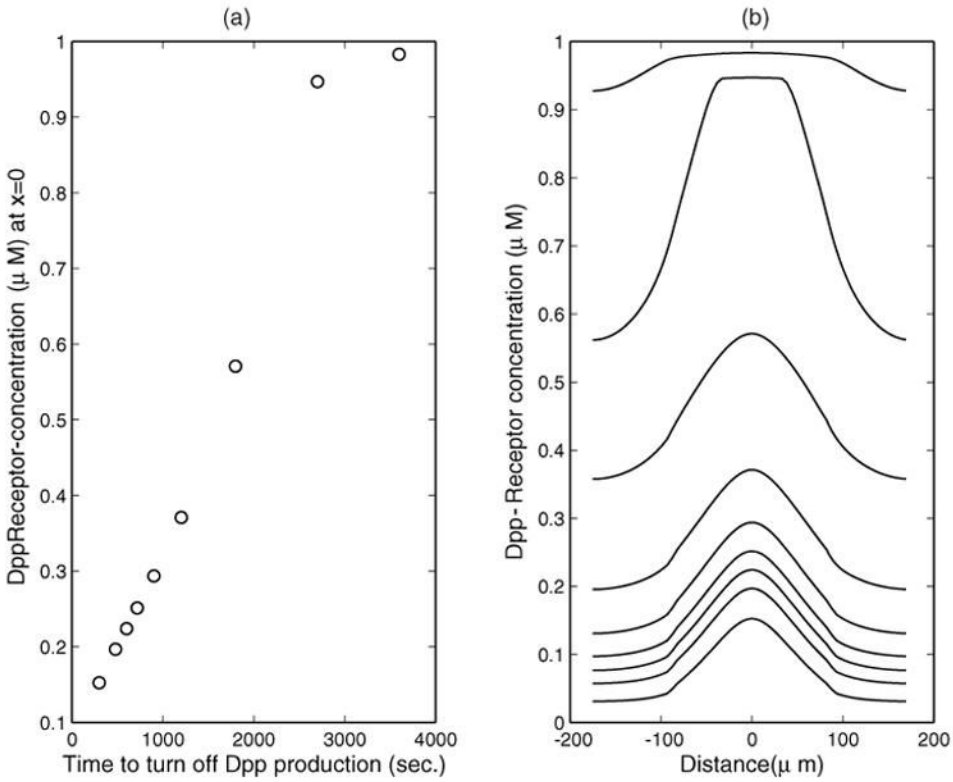

Fig. 6.

$\bar{v}_L$ is set to zero at different times. (a) [LR] at the dorsal midline at steady state as a function of the time for turning off $\bar{v}_L$; (b) [LR] at steady states as a function of space for different times of turning off $\bar{v}_L$, as shown in (a). Other parameters are as in Figure 3 except that $K_{deg} = 0$.

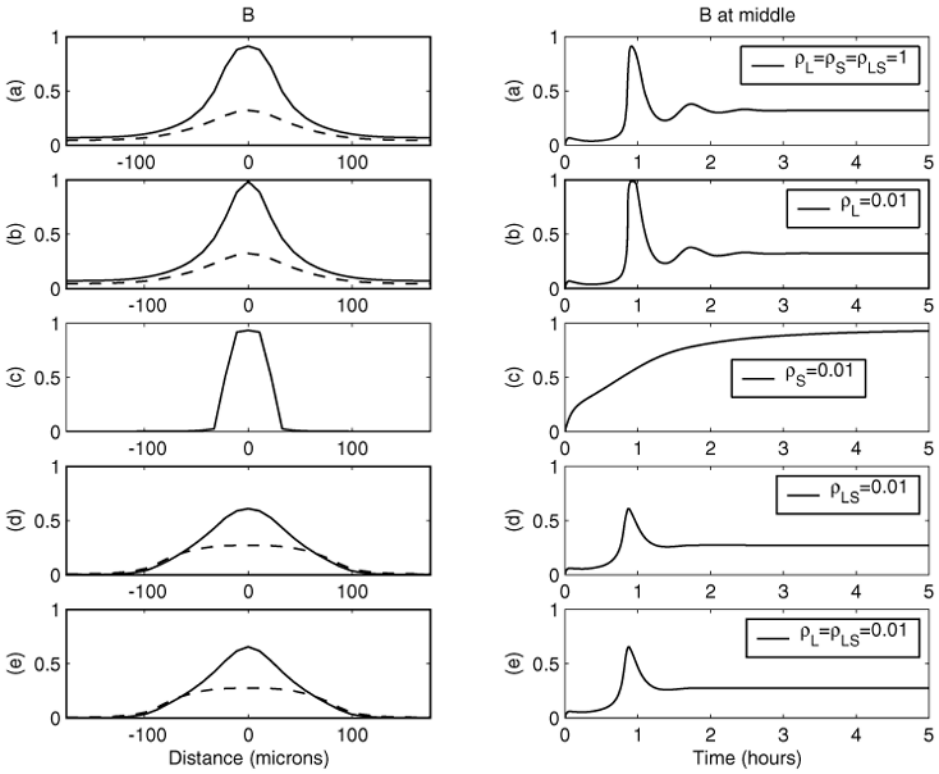

Fig. 7.

Effect of smaller diffusion constants on the transient peak and steady state. For the left-hand panels, solid line: transient peak; dotted line: steady state. Parameters are as in Figure 3 except for diffusion constants.

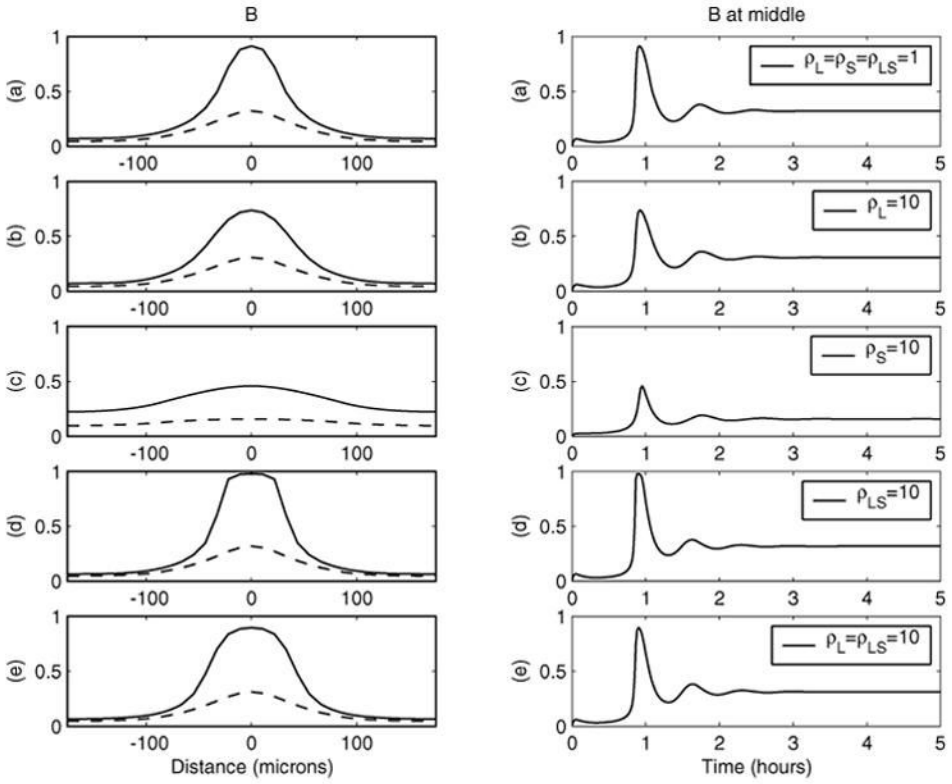

Fig. 8.

Effect of larger diffusion constants on the transient peak and steady state. For the left-hand panels, solid line: transient peak; dotted line: steady state. Parameters are as in Figure 3 except for diffusion constants.